

$O(\alpha_s)$ corrections to polarized top quark decay into a charged Higgs $t(\uparrow) \rightarrow H^+ + b$

A. Kadeer, J.G. Körner and M.C. Mauser

Institut für Physik, Johannes Gutenberg-Universität
Staudinger Weg 7, D-55099 Mainz, Germany

Abstract

We calculate the $O(\alpha_s)$ radiative corrections to polarized top quark decay into a charged Higgs boson and a massive bottom quark in two variants of the two-Higgs-doublet model. The radiative corrections to the polarization asymmetry of the decay may become as large as 25%. We provide analytical formulae for the unpolarized and polarized rates for $m_b \neq 0$ and for $m_b = 0$. For $m_b = 0$ our closed-form expressions for the unpolarized and polarized rates become rather compact.

1 Introduction

The purpose of this paper is the evaluation of the first order QCD corrections to the decay of a polarized top quark into a charged Higgs boson and a bottom quark. Highly polarized top quarks will become available at hadron colliders through single top production, which occurs at the 33 % level of the top quark pair production rate [1, 2]. Future e^+e^- – colliders will also be copious sources of polarized top quark pairs. The polarization of these can easily be tuned through the availability of polarized beams [3, 4]. Measurements of the decay rate and the polarization asymmetry in the decay $t(\uparrow) \rightarrow H^+ + b$ will be important for future tests of the Higgs coupling in the minimal supersymmetric standard model (MSSM).

The $O(\alpha_s)$ corrections to the decay rate $t \rightarrow H^+ + b$ have been calculated previously in [5, 6, 7, 8, 9, 10, 11, 12, 13], and have been found to be important. The present paper provides the first calculation of the $O(\alpha_s)$ radiative corrections to the polarization asymmetry in polarized top quark decay $t(\uparrow) \rightarrow H^+ + b$. Depending on the value of $\tan \beta$ and the mass of the charged Higgs boson the radiative corrections to the polarization asymmetry can become quite large (up to 25 %) in one variant of the two-Higgs-doublet model and must therefore be included in a decay analysis.

The decay $t \rightarrow H^+ + b$ is analyzed in the rest frame of the top quark (see Fig. 1). The three-momentum \vec{q} of the H^+ boson points into the direction of the positive z -axis. The polar angle θ_P is defined as the angle between the polarization vector \vec{P} of the top quark and the z -axis.

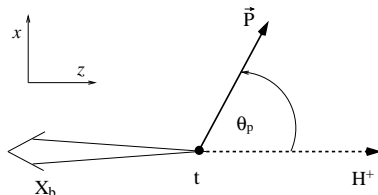


Figure 1: Definition of the polar angle θ_P . \vec{P} is the polarization vector of the top quark.

In terms of the unpolarized rate Γ and the polarized rate Γ^P the differential decay rate is given by

$$\frac{d\Gamma}{d\cos\theta_P} = \frac{1}{2} \left(\Gamma + P \Gamma^P \cos\theta_P \right) = \frac{1}{2} \Gamma \left(1 + P \alpha_H \cos\theta_P \right), \quad (1)$$

where P is the degree of polarization. The polarization asymmetry α_H is defined by $\alpha_H = \Gamma^P/\Gamma$. Alternatively one can define a forward-backward asymmetry A_{FB} by writing

$$A_{FB} = \frac{\Gamma_F - \Gamma_B}{\Gamma_F + \Gamma_B}, \quad (2)$$

where Γ_F and Γ_B are the rates into the forward and backward hemispheres, respectively. The two measures are related by $A_{FB} = \frac{1}{2}P\alpha_H$. In our numerical results we shall always set $P = 1$ for simplicity.

Technical details of our calculation can be found in [14]. As in [14] we use dimensional regularization ($D = 4 - 2\omega$ with $\omega \ll 1$) to regularize the ultraviolet divergences of the virtual corrections. We regularize the infrared divergences in the virtual one-loop and the real gluon emissions (tree-graph) corrections by introducing a finite (small) gluon mass $m_g \neq 0$ in the gluon propagator. In the tree-graph corrections the phase space boundary becomes deformed away from the IR singular point through the introduction of a (small) gluon mass. The logarithmic gluon mass dependence resulting from the regularization procedure cancels out when adding the virtual and tree-graph contributions. We have checked consistency with the Goldstone boson equivalence theorem which, in the limit $m_{W^+}/m_t \rightarrow 0$ and $m_{H^+}/m_t \rightarrow 0$, relates Γ and Γ^P for $t \rightarrow H^+ + b$ to the unpolarized and polarized longitudinal rates Γ_L and Γ_L^P in the decay $t \rightarrow W^+ + b$ calculated in [14].

2 Born term results

The coupling of the charged Higgs boson to the top and bottom quark in the MSSM can either be expressed as a superposition of scalar and pseudoscalar coupling factors or as a superposition of right- and left-chiral coupling factors. The Born term amplitude is thus given by

$$\mathcal{M}_0 = \bar{u}_b(a\mathbb{1} + b\gamma_5)u_t = \bar{u}_b \left\{ g_t \frac{\mathbb{1} + \gamma_5}{2} + g_b \frac{\mathbb{1} - \gamma_5}{2} \right\} u_t, \quad (3)$$

where $a = \frac{1}{2}(g_t + g_b)$ and $b = \frac{1}{2}(g_t - g_b)$. The inverse relation reads $g_t = a + b$ and $g_b = a - b$.

If the top quark mass m_t , bottom quark mass m_b and the charged Higgs boson mass m_{H^+} satisfy $m_t > m_{H^+} + m_b$, the top quark decay $t \rightarrow H^+ + b$ is possible in the MSSM. In order to avoid flavor changing neutral currents (FCNC) the generic Higgs coupling to all quarks has to be restricted. In the notation of [15] in model 1 the doublet H_1 couples to all bosons and the doublet H_2 couples to all quarks. This leads to the coupling factors

$$\boxed{\text{model 1:}} \quad a = \frac{g_w}{2\sqrt{2}m_W} V_{tb}(m_t - m_b) \cot \beta, \quad (4a)$$

$$b = \frac{g_w}{2\sqrt{2}m_W} V_{tb}(m_t + m_b) \cot \beta, \quad (4b)$$

where V_{tb} is the CKM-matrix element and $\tan \beta = v_2/v_1$ is the ratio of the vacuum expectation values of the two electrically neutral components of the two Higgs doublets. The weak coupling factor g_w is related to the usual Fermi coupling constant G_F by $g_w^2 = 4\sqrt{2}m_W^2 G_F$.

In model 2, the doublet H_1 couples to the right-chiral down-type quarks and the doublet H_2 couples to the right-chiral up-type quarks. Model 2 leads to the coupling factors

$$\boxed{\text{model 2:}} \quad a = \frac{g_w}{2\sqrt{2}m_W} V_{tb}(m_t \cot \beta + m_b \tan \beta), \quad (5a)$$

$$b = \frac{g_w}{2\sqrt{2}m_W} V_{tb}(m_t \cot \beta - m_b \tan \beta). \quad (5b)$$

Since $m_b \ll m_t$ the b mass can always be safely neglected in model 1. In model 2 the left-chiral coupling term proportional to $m_b \tan \beta$ can become comparable to the right-chiral coupling term $m_t \cot \beta$ when $\tan \beta$ becomes large. One cannot therefore naively set $m_b = 0$ in all expressions in model 2. One has to distinguish between the cases in which the scale of m_b is set by $m_t \cot^2 \beta$ and those in which the scale of m_b is set by m_t . In the former case one has to keep m_b finite. In the latter case m_b can safely be set to zero except for logarithmic terms proportional to $\ln(m_b/m_t)$ that appear in the NLO calculation. Keeping this distinction results in very compact closed-form expressions for the radiatively corrected unpolarized and polarized rates which we shall list in the main text. We shall, however, also present general $m_b \neq 0$ results along with the $m_b = 0$ results. It is quite evident that one has to use the $m_b \neq 0$ expressions for charged Higgs masses close to the top quark mass.

For the amplitude squared one obtains

$$|\mathcal{M}_0|^2 = \sum_{s_b} \mathcal{M}_0^\dagger \mathcal{M}_0 = 2(p_t \cdot p_b)(a^2 + b^2) + 2(a^2 - b^2)m_t m_b + 4abm_t(p_b \cdot s_t), \quad (6)$$

where p_t and p_b are the four-momenta of the top and bottom quarks. s_t denotes the polarization four-vector of the top quark. Accordingly the unpolarized and polarized Born term rates read

$$\Gamma_{Born} = \frac{m_t \sqrt{\lambda}}{16\pi} \left[(a^2 + b^2)(1 - y^2 + \epsilon^2) + 2(a^2 - b^2)\epsilon \right], \quad (7a)$$

$$\Gamma_{Born}^P = \frac{m_t \sqrt{\lambda}}{16\pi} 2ab\sqrt{\lambda}, \quad (7b)$$

where we have used the abbreviations $\lambda = \lambda(1, y^2, \epsilon^2)$ with the Källén function $\lambda(a, b, c) := a^2 + b^2 + c^2 - 2(ab + bc + ca)$. The scaled masses y and ϵ are defined as

$$y := \frac{m_{H^+}}{m_t}, \quad \epsilon := \frac{m_b}{m_t}. \quad (8)$$

As mass values we take $m_b = 4.8 \text{ GeV}$ and $m_t = 175 \text{ GeV}$ such that $\epsilon = 0.027$. For later use we register that the factor $\text{PS}_2 = \sqrt{\lambda}/(16\pi m_t)$ is a two-body phase space factor.

In the limit $m_b \rightarrow 0$ the unpolarized and polarized Born term rates simplify to

$$\lim_{m_b \rightarrow 0} \Gamma_{Born} = (a^2 + b^2) \left\{ 1 + \frac{a^2 - b^2}{a^2 + b^2} \frac{2\epsilon}{1 - y^2} \right\} \hat{\Gamma}, \quad (9a)$$

$$\lim_{m_b \rightarrow 0} \Gamma_{Born}^P = 2ab \hat{\Gamma}, \quad (9b)$$

where

$$\hat{\Gamma} = \frac{m_t(1 - y^2)^2}{16\pi}. \quad (10)$$

Eqs. (9a) and (9b) are quite useful for a discussion of the qualitative behavior of the unpolarized and polarized rates in the two models as long as one is not too close to the kinematical limit $y = 1 - \epsilon$. In fact, for most of the y -region away from the endpoint $y = 1 - \epsilon$, Eqs. (9a) and (9b) are an excellent approximation to Eqs. (7a) and (7b).

For model 1 one has $(a^2 - b^2)/(a^2 + b^2) = -2\epsilon/(1 + \epsilon^2)$ and thus the second term in the curly brackets of Eq. (9a) can be safely dropped for $\epsilon \rightarrow 0$ except when y gets close to $1 - \epsilon$. For model 2 one has $(a^2 - b^2)/(a^2 + b^2) = 2\epsilon/(\cot^2 \beta + \epsilon^2 \tan^2 \beta)$, which, when combined with the factor 2ϵ in Eq. (9a), can become as large as $\mathcal{O}(5\%)$ for e.g. $\tan \beta \approx 5$. Since this is further multiplied by $(1 - y^2)^{-1}$ we shall therefore always keep the second term in the curly brackets of Eq. (9a) in model 2 when making use of the $m_b \rightarrow 0$ approximation.

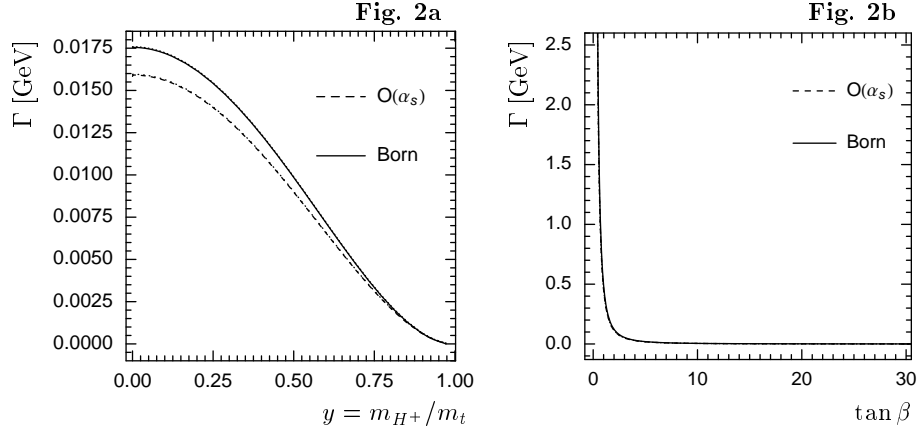


Figure 2: Unpolarized decay rate for model 1 as a function of $y = m_{H^+}/m_t$ (Fig. 2a; $\tan \beta = 10$) and as a function of $\tan \beta$ (Fig. 2b; $m_{H^+} = 120$ GeV). Other parameters are $m_b = 4.8$ GeV, $m_t = 175$ GeV. The barely visible dotted lines show the corresponding $m_b \rightarrow 0$ curves.

In model 1 the y dependence of the unpolarized and polarized rate is essentially determined by the $(1 - y^2)^2$ dependence of the overall factor $\hat{\Gamma}$ in Eqs. (9a) and (9b). The overall scales of both the unpolarized and polarized rates are set by $\cot^2 \beta$, which means that their ratio, the polarization asymmetry α_H , is independent of the value of $\tan \beta$.

In Fig. 2a we show the unpolarized rate as a function of $y = m_{H^+}/m_t$ for $\tan \beta = 10$, which exhibits the $(1 - y^2)^2$ dependence of $\hat{\Gamma}$ in Eq. (10). Compared to the partial Born term rate $\Gamma_{t \rightarrow W^+ b} = 1.56$ GeV the rate into a charged Higgs is generally quite small except for small $\tan \beta$ values. This can also be seen in Fig. 2b where we plot the rate

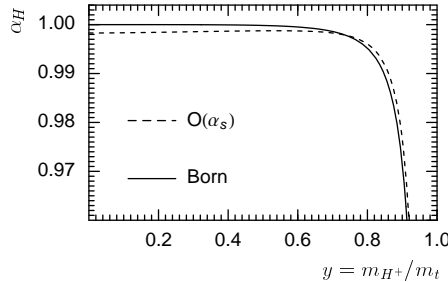


Figure 3: Polarization asymmetry α_H for model 1 with $m_b = 4.8$ GeV and $m_t = 175$ GeV as a function of m_{H^+}/m_t . No value of $\tan \beta$ is given since α_H does not depend on $\tan \beta$ in model 1.

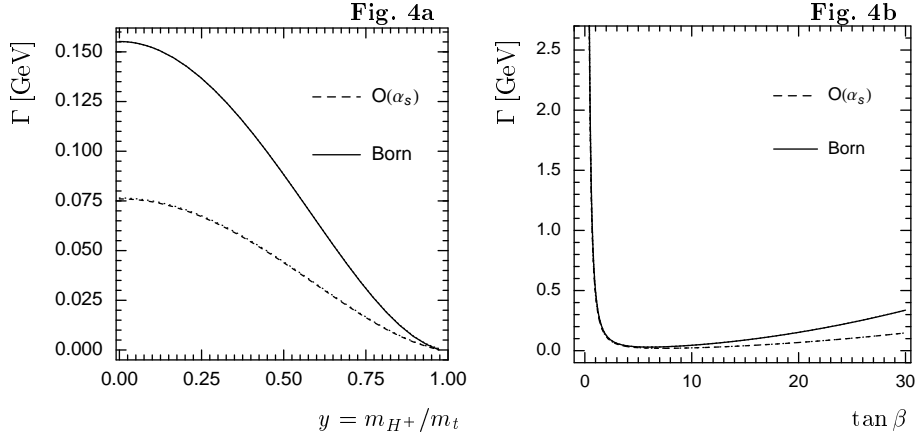


Figure 4: Unpolarized decay rate for model 2 as a function of $y = m_{H^+}/m_t$ (Fig. 4a; $\tan \beta = 10$) and as a function of $\tan \beta$ (Fig. 4b; $m_{H^+} = 120$ GeV). Other parameters are $m_b = 4.8$ GeV, $m_t = 175$ GeV. The barely visible dotted lines show the corresponding $m_b \rightarrow 0$ curves.

as a function of $\tan \beta$ for a sample value $m_{H^+} = 120$ GeV, which shows the $1/\tan^2 \beta$ fall-off behavior of the overall factor $(a^2 + b^2) \propto 1/\tan^2 \beta$ in the rate expression Eq. (9a). The rate into a charged Higgs can be seen to be quite small for $\tan \beta$ values exceeding $\tan \beta = 2$. One finds equality of the partial rates into a W^+ and H^+ only at $\tan \beta = 0.56$ for $m_{H^+} = 120$ GeV. Such a small $\tan \beta$ value is excluded by the indirect limits in the $(m_{H^\pm}, \tan \beta)$ plane [16].

In Fig. 3 we display the behavior of the polarization asymmetry α_H as a function of $y = m_{H^+}/m_t$. As expected from the flat behavior of $(a^2 + b^2)/(2ab)$ the polarization asymmetry α_H stays very close to its maximal value $\alpha_H \approx 1$ except for the endpoint region $y \rightarrow (1 - \epsilon)$. At $y = 1 - \epsilon$ the polarization asymmetry drops to $\alpha_H = 0$ (not shown). We do not show a plot of the polarization asymmetry as a function of $\tan \beta$, because, as mentioned before, the polarization asymmetry does not depend on $\tan \beta$ for model 1.

The y and $\tan \beta$ dependence of model 2 is somewhat more involved. The overall scales for the unpolarized and polarized rates are now set by $(\cot^2 \beta \pm \epsilon^2 \tan^2 \beta)$, respectively. The y dependence of both the unpolarized and polarized rates is again close to the $\epsilon \rightarrow 0$ limit since they are dominated by the $(1 - y^2)^2$ behavior of $\hat{\Gamma}$. However, in the case of the unpolarized rate, the y dependence is slightly modified by the curly brackets in Eq. (9a). In Fig. 4a we display the dependence of the rate on $y = m_{H^+}/m_t$ where we take again $\tan \beta = 10$ as a numerical example. As in model 1 the functional behavior is again

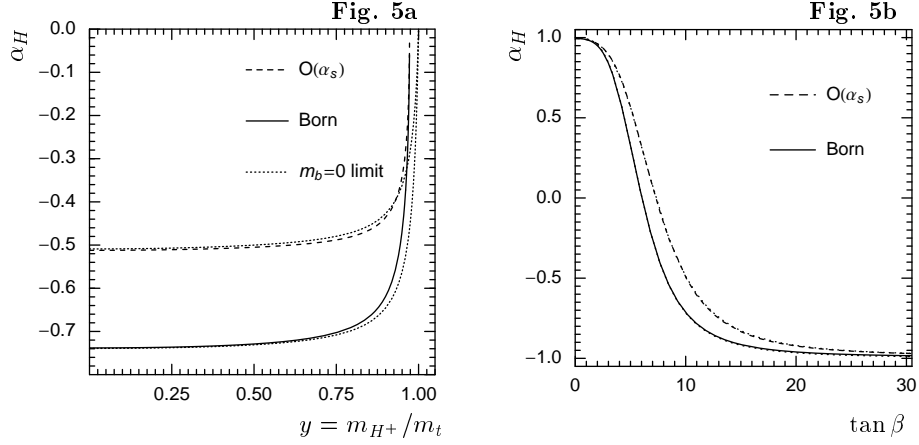


Figure 5: Polarization asymmetry α_H for model 2 with $m_b = 4.8$ GeV and $m_t = 175$ GeV as a function of m_{H^+}/m_t (Fig. 5a, $\tan\beta = 10$) and as function of $\tan\beta$ (Fig. 5b, $m_{H^+} = 120$ GeV). The dotted lines (barely visible in Fig. 5b) show the corresponding $m_b \rightarrow 0$ curves.

essentially determined by the overall $(1 - y^2)^2$ behavior of Eq. (9a) except for the region close to the endpoint where the second term in the curly brackets of Eq. (9a) comes into play. The rate is largest for $m_{H^+} = 0$ and drops to zero towards the phase space boundary $y = 1 - \epsilon$. The model 2 rate is considerably larger than the model 1 rate, depending, of course on the value of $\tan\beta$. This is because of the overall rate factor $(a^2 + b^2)$ whose model 2/model 1 ratio

$$\frac{(a^2 + b^2)|_{\text{model 2}}}{(a^2 + b^2)|_{\text{model 1}}} = \frac{(1 + \epsilon^2 \tan^4 \beta)}{(1 + \epsilon^2)} \quad (11)$$

is larger than 1 for $\tan\beta > 1$. For example, for $\tan\beta = 10$ and $\epsilon = 0.027$ one has $(a^2 + b^2)|_{\text{model 2}}/(a^2 + b^2)|_{\text{model 1}} = 8.28$. The second term in the curly brackets of Eq. (9a) gives a much smaller enhancement. For example, for $y = 0$, $\tan\beta = 10$ and $\epsilon = 0.027$, the enhancement due to the second term in the curly brackets of Eq. (9a) is only 3.5%. Nevertheless, the model 2 rate is still small compared to the Standard Model Born term rate $\Gamma_{t \rightarrow W^+ + b} = 1.56$ GeV for most of the range of $\tan\beta$ value.

In Fig. 4b we plot the $\tan\beta$ dependence of the unpolarized rate for $m_{H^+} = 120$ GeV. The $\tan\beta$ dependence of the rate is determined by the overall $\tan\beta$ -dependent factor $(a^2 + b^2) \propto (1 + \epsilon^2 \tan^4 \beta)/\tan^2 \beta$ with a slight modification due to the second term in the curly brackets in Eq. (9a). As in model 1 the rates drop very fast at the origin for small $\tan\beta$ values due to the dominant $1/\tan^2 \beta$ behavior of the overall factor $(a^2 + b^2)$. Contrary to model 1 the rate rises quadratically for larger $\tan\beta$ values after going through

a minimum at $\tan \beta \approx 7$ due to the $\tan^2 \beta$ term in the overall rate factor. It reaches equality with the Standard Model Born term rate $\Gamma_{t \rightarrow W^+ + b} = 1.56 \text{ GeV}$ at $\tan \beta = 0.56$ and $\tan \beta = 64.83$. Again these values of $\tan \beta$ are excluded by the indirect limits in the $(m_{H^\pm}, \tan \beta)$ plane [16].

All of what has been stated in the last paragraph does not change qualitatively but quantitatively if one uses a running mass for the bottom quark instead of a fixed pole mass. At one-loop running one would then have $\bar{m}_b(m_t) = 1.79 \text{ GeV}$ and $\epsilon = \bar{m}_b(m_t)/m_t = 0.010$ instead of $\epsilon = 0.027$. The main effect would be a reduction of the model 2 rate for larger values of $\tan \beta$ due to the overall factor $(a^2 + b^2)$. For example, for $\tan \beta = 10$ one would have a rate reduction by a factor of 0.24 due to the factor $(a^2 + b^2)$ when one uses a running bottom quark mass instead of a fixed pole mass.

The main qualitative features of the behavior of the polarization asymmetry α_H in model 2 can again be understood from the $m_b \rightarrow 0$ behavior of α_H given by the ratio of Eq. (9b) and Eq. (9a). One has

$$\lim_{m_b \rightarrow 0} \alpha_H = \frac{1 - \epsilon^2 \tan^4 \beta}{1 + \epsilon^2 \tan^4 \beta} \left\{ 1 + \frac{4\epsilon}{(1 - y^2)} \frac{\epsilon \tan^2 \beta}{1 + \epsilon^2 \tan^4 \beta} \right\}^{-1}. \quad (12)$$

The y dependence comes only from the second term in the curly brackets of Eq. (12) and is therefore not very pronounced. This can be seen in Fig. 5a, where we show a plot of the polarization asymmetry α_H as a function of y for $\tan \beta = 10$ in model 2. α_H is large and negative with only little dependence on the Higgs mass except for the region close to the phase space boundary $y = 1 - \epsilon$ where α_H approaches zero. α_H is negative due to the fact that the numerator factor $(1 - \epsilon^2 \tan^4 \beta)$ is negative for $\tan \beta = 10$. For the smaller y values the functional behavior is dominated by the first term in the curly brackets of Eq. (12), and therefore the curve is rather flat. Towards $y = 1 - \epsilon$ the second term in the curly bracket of Eq. (12) becomes dominant and the curve bends up and finally reaches zero at $y = 1 - \epsilon$. The $\epsilon = 0$ approximation can be seen to be quite good up to $y \approx 0.7$. In Fig. 5b we show a plot of the polarization asymmetry α_H as a function of $\tan \beta$ for $m_{H^+} = 120 \text{ GeV}$, i.e. $y = 0.69$. Contrary to model 1, α_H shows a strong dependence on the value of $\tan \beta$. α_H is positive/negative for small/large values of $\tan \beta$ and goes through zero for $\tan \beta = \sqrt{m_t/m_b} = 6.04$ close to where the rate has a minimum. Beyond the zero position α_H rapidly approaches values close to $\alpha_H = -1$. Both Figs. 5a and 5b show that $m_b \rightarrow 0$ is a very good approximation. At the scale of the figures the dotted curve cannot be discerned from the exact full curves.

3 Virtual corrections

The virtual one-loop corrections to the (tH^+b) -vertex exhibit both IR- and UV-singularities. As mentioned before, the UV-singularities are regularized in $D = 4 - 2\omega$ dimensions, whereas the IR-singularities are regularized by a small gluon mass m_g . The scaled gluon mass is denoted by

$$\Lambda := \frac{m_g}{m_t}. \quad (13)$$

The renormalization of the UV-singularities is done in the “on-shell” scheme.

The renormalized amplitude of the virtual corrections in the right- and left-chiral representation can be written as

$$\mathcal{M}_{loop} = \bar{u}_b \left\{ \left(a\mathbb{1} + b\gamma_5 \right) \Lambda_1 + a\Lambda_2 + \delta\Lambda \right\} u_t, \quad (14)$$

where the functions Λ_1 and Λ_2 read ($C_F = \frac{4}{3}$)

$$\begin{aligned} \Lambda_1 &= \frac{\alpha_s}{2\pi} C_F \left\{ (m_t^2 + m_b^2 - m_H^2) C_0 - \left[2m_t^2 - m_H^2 + m_b(m_t + m_b) \right] C_1 \right. \\ &\quad \left. - \left[2m_b^2 - m_H^2 + m_t(m_t + m_b) \right] C_2 + 2B_0 - 1 \right\}, \\ \Lambda_2 &= \frac{\alpha_s}{2\pi} C_F \left\{ 2m_b m_t (C_1 + C_2) \right\}. \end{aligned} \quad (15a)$$

The standard one-loop integrals B_0 , C_0 , C_1 and C_2 are given in Appendix A. After a linear transformation these loop functions can be seen to agree with Eqs. (8) and (9) in Ref. [7]. Following Refs. [6, 7, 10, 17] the counter term of the vertex is given by

$$\begin{aligned} \delta\Lambda &= (a+b) \frac{\mathbb{1} + \gamma_5}{2} \left(\frac{1}{2}(Z_2^t - 1) + \frac{1}{2}(Z_2^b - 1) - \frac{\delta m_t}{m_t} \right) \\ &\quad + (a-b) \frac{\mathbb{1} - \gamma_5}{2} \left(\frac{1}{2}(Z_2^t - 1) + \frac{1}{2}(Z_2^b - 1) - \frac{\delta m_b}{m_b} \right). \end{aligned} \quad (16)$$

In the “on-shell” scheme the wavefunction renormalization constant Z_2^q and the mass renormalization constant δm_q can be calculated from the renormalized QCD self-energy $\Sigma_q(p)$ of the quarks $q = t, b$. The evaluation of the two conditions $\Sigma_q(p)|_{\not{p}=m_q} = 0$ and $\partial\Sigma_q(p)/\partial\not{p}|_{\not{p}=m_q} = 0$ lead to the following renormalization constants

$$Z_2^q = 1 - \frac{\alpha_s}{4\pi} C_F \left[\frac{1}{\omega} - \gamma_E + \ln \frac{4\pi\mu^2}{m_q^2} + 2 \ln \frac{m_g^2}{m_q^2} + 4 \right], \quad (17a)$$

$$\delta m_q = \frac{\alpha_s}{4\pi} C_F m_q \left(\frac{3}{\omega} - 3\gamma_E + 3 \ln \frac{4\pi\mu^2}{m_q^2} + 4 \right), \quad (17b)$$

where p is the four-momentum and m_q is the mass of the relevant quark.

Putting everything together the virtual one-loop contributions to the unpolarized and polarized rates read ($\lambda = \lambda(1, y^2, \epsilon^2)$)

$$\begin{aligned} \Gamma_{loop} &= \Gamma_{Born} \left(Z_2^t - 1 + Z_2^b - 1 - \frac{\delta m_t}{m_t} - \frac{\delta m_b}{m_b} + 2\Lambda_1 \right) \\ &\quad + \frac{m_t \sqrt{\lambda}}{16\pi} \left(2a^2 \Lambda_2 ((1 + \epsilon)^2 - y^2) - 2ab(1 - y^2 + \epsilon^2) \left(\frac{\delta m_t}{m_t} - \frac{\delta m_b}{m_b} \right) \right), \\ \Gamma_{loop}^P &= \Gamma_{Born}^P \left(Z_2^t - 1 + Z_2^b - 1 - \frac{\delta m_t}{m_t} - \frac{\delta m_b}{m_b} + 2\Lambda_1 + \Lambda_2 \right) \\ &\quad + \frac{m_t \sqrt{\lambda}}{16\pi} (a^2 + b^2) \sqrt{\lambda} \left(\frac{\delta m_b}{m_b} - \frac{\delta m_t}{m_t} \right). \end{aligned} \quad (18a)$$

The renormalized virtual one-loop correction to the unpolarized rate (18a) is in agreement with Ref. [7]. The result for the virtual one-loop correction to the polarized rate is new. Note that the infrared divergent terms residing in the renormalization factor Z_2^q and in the integral term C_0 in Λ_1 are proportional to the Born term rates Γ_{Born} and Γ_{Born}^P , respectively.

4 Tree-graph contributions

The $\mathcal{O}(\alpha_s)$ real gluon emission (tree-graph) amplitude reads

$$\mathcal{M}_{tree} = g_s \frac{\lambda^a}{2} \bar{u}_b \left\{ \frac{2p_t^\sigma - \not{k}\gamma^\sigma}{2k \cdot p_t} - \frac{2p_b^\sigma + \gamma^\sigma \not{k}}{2k \cdot p_b} \right\} \left(a\mathbb{1} + b\gamma_5 \right) u_t \varepsilon_\sigma^*(k, \lambda), \quad (19)$$

where the first and second terms in the curly brackets refer to real gluon emission from the top quark and the bottom quark, respectively. The four-momenta of the charged

Higgs and the gluon are denoted by q and k . The polarization vector of the gluon with momentum k and spin λ is denoted by $\varepsilon(k, \lambda)$.

In the square of the tree-graph amplitude the terms without gluon momentum in the numerator, i.e. the terms proportional to p_t and p_b in the numerator lead to IR-divergences, which are regulated by a small gluon mass. Separating these terms will split the squared tree-graph amplitude into an IR-convergent part $|\mathcal{M}_{tree}^{conv}|^2$ and an IR-divergent part proportional to the soft gluon factor $|\mathcal{M}|_{SGF}^2$ as follows:

$$|\mathcal{M}_{tree}|^2 = |\mathcal{M}_{tree}^{conv}|^2 + |\widetilde{\mathcal{M}}_0|^2 |\mathcal{M}|_{SGF}^2 \quad (20)$$

where the factor $|\widetilde{\mathcal{M}}_0|^2$ and the universal soft gluon (or eikonal) factor $|\mathcal{M}|_{SGF}^2$ are given by

$$|\mathcal{M}|_{SGF}^2 = -4\pi\alpha_s C_F \left[\frac{m_t^2}{(k \cdot p_t)^2} + \frac{m_b^2}{(k \cdot p_b)^2} - 2 \frac{p_b \cdot p_t}{(k \cdot p_b)(k \cdot p_t)} \right], \quad (21)$$

$$|\widetilde{\mathcal{M}}_0|^2 = 2(p_t \cdot p_b)(a^2 + b^2) + 2(a^2 - b^2)m_t m_b + 4abm_t(p_b \cdot s_t). \quad (22)$$

Note that the factor $|\widetilde{\mathcal{M}}_0|^2$ has the same analytical form as the squared Born term amplitude $|\mathcal{M}_0|^2$ listed in Eq. (6) but must of course be evaluated for $p_t = p_b + q + k$, i.e. one has $|\widetilde{\mathcal{M}}_0|^2(k=0) = |\mathcal{M}_0|^2$.

When integrating $|\widetilde{\mathcal{M}}_0|^2 |\mathcal{M}|_{SGF}^2$ one has to take care of the fact that both terms in the product depend on the gluon momentum. Since $(|\widetilde{\mathcal{M}}_0|^2 - |\mathcal{M}_0|^2) |\mathcal{M}|_{SGF}^2$ is convergent and thus can be integrated without a gluon mass regulator, we further isolate the IR-divergent part by writing

$$|\mathcal{M}_{tree}|^2 = \left\{ |\mathcal{M}_{tree}^{conv}|^2 + \left(|\widetilde{\mathcal{M}}_0|^2 - |\mathcal{M}_0|^2 \right) |\mathcal{M}|_{SGF}^2 \right\} + |\mathcal{M}_0|^2 |\mathcal{M}|_{SGF}^2, \quad (23)$$

where the gluon momentum dependence in the IR divergent last term of (23) solely resides in the soft gluon factor $|\mathcal{M}|_{SGF}^2$.

The same universal soft gluon factor $|\mathcal{M}|_{SGF}^2$ appears in the calculation of the radiative corrections to $t \rightarrow W^+ + b$. We can therefore take the result of its phase space integration (with $m_g \neq 0$) from Eq. (63) in Ref. [14].

The IR-convergent part of $|\mathcal{M}_{tree}|^2$ is thus given by

$$\begin{aligned}
|\mathcal{M}_{tree}^{conv}|^2 + \left(|\widetilde{\mathcal{M}}_0|^2 - |\mathcal{M}_0|^2\right) |\mathcal{M}|_{SGF}^2 = 8\pi\alpha_s C_F \frac{k \cdot q}{(k \cdot p_t)(k \cdot p_b)} & \left\{ (a^2 + b^2)(k \cdot q) + \right. \\
-2abm_t \left[\left(\frac{m_t^2 + m_{H^+}^2 - m_b^2}{2k \cdot p_t} - 1 - \frac{m_{H^+}^2}{k \cdot q} \right) (k \cdot s_t) + (q \cdot s_t) \right. & \\
\left. \left. + \left(\frac{m_t^2}{k \cdot p_t} - \frac{m_b^2}{k \cdot p_b} - 2 - \frac{m_{H^+}^2}{k \cdot q} \right) \left((q \cdot s_t) - (q \cdot s_t)|_{k=0} \right) \right] \right\}. & \quad (24)
\end{aligned}$$

It is quite remarkable that the unpolarized and polarized pieces of the convergent tree-level contribution are proportional to $(a^2 + b^2)$ and $2ab$, respectively.

The phase space integration is done with respect to the gluon energy k_0 and the H^+ boson energy E_{H^+} , where the k_0 integration is done first. It is convenient to introduce the scaled invariant mass of the bottom quark-gluon system $z = \frac{(p_b+k)^2}{m_t^2}$. Using the relation $E_{H^+} = (m_t^2 + m_{H^+}^2 - m_t^2 z)/(2m_t)$ we change to the integration variable z .

Note that the last line of the Eq. (24) comes from the term $\left(|\widetilde{\mathcal{M}}_0|^2 - |\mathcal{M}_0|^2\right) |\mathcal{M}|_{SGF}^2$ in Eq. (23). The relevant scalar products are evaluated in the top quark rest frame. They read

$$(q \cdot s_t) = -\frac{1}{2} \sqrt{\lambda(1, y^2, z)} m_t \cos \theta_P, \quad (25)$$

$$(q \cdot s_t)|_{k=0} = -\frac{1}{2} \sqrt{\lambda(1, y^2, \epsilon^2)} m_t \cos \theta_P. \quad (26)$$

After k_0 integration the remaining phase space integrations can be reduced to the following classes of basic integrals ($\lambda' = \lambda(1, y^2, z)$):

$$R(n) := \int dz \frac{1}{(z - \epsilon^2) \sqrt{\lambda'^n}}, \quad (27a)$$

$$R(m, n) := \int dz \frac{z^m}{\sqrt{\lambda'^n}}, \quad (27b)$$

$$S(n) := \int dz \frac{1}{(z - \epsilon^2) \sqrt{\lambda'^n}} \ln \left[\frac{1 - y^2 + z + \sqrt{\lambda'}}{1 - y^2 + z - \sqrt{\lambda'}} \right], \quad (27c)$$

$$S(m, n) := \int dz \frac{z^m}{\sqrt{\lambda'^n}} \ln \left[\frac{1 - y^2 + z + \sqrt{\lambda'}}{1 - y^2 + z - \sqrt{\lambda'}} \right], \quad (27d)$$

with the integration limits $\epsilon^2 \leq z \leq (1-y)^2$. The basic integrals needed in the present application are listed in Appendix C.

Finally, the unpolarized and polarized tree-graph contributions read

$$\Gamma_{tree} = -\frac{1}{4\pi m_t} \left[\frac{\alpha_s}{4\pi} C_F m_t^2 (a^2 + b^2) \left\{ \frac{3}{4} R(0, -1) + \frac{\epsilon^2 (1-y^2)}{4} R(-2, -1) \right. \right. \\ \left. \left. - \frac{1-y^2+3\epsilon^2}{4} R(-1, -1) + \frac{1}{2} \epsilon^2 S(0, 0) - \frac{1}{2} S(1, 0) \right\} + \text{PS}_2^{-1} \Gamma_{Born} S(\Lambda) \right], \quad (28a)$$

and

$$\Gamma_{tree}^P = -\frac{1}{4\pi m_t} \left[\frac{\alpha_s}{4\pi} C_F m_t^2 2ab \left\{ -2\sqrt{\lambda} R(-1) + 2\lambda R(0) + \frac{1}{4} (1-y^2)^2 \epsilon^2 R(-2, 0) \right. \right. \\ \left. \left. - \frac{1}{4} \left((1-y^2)^2 + 2(3-y^2)\epsilon^2 \right) R(-1, 0) - \frac{1}{4} (2+10y^2-\epsilon^2) R(0, 0) + \frac{7}{4} R(1, 0) \right. \right. \\ \left. \left. + (1-y^2+\epsilon^2) \sqrt{\lambda} S(0) - (1-y^2+\epsilon^2)\lambda S(1) + \sqrt{\lambda} S(0, 0) + \frac{1}{2} \left(4y^2(1-y^2) \right. \right. \right. \\ \left. \left. \left. + (7+5y^2)\epsilon^2 - 2\epsilon^4 \right) S(0, 1) - \frac{1}{2} (3-3y^2+\epsilon^2) S(1, 1) - \frac{1}{2} S(2, 1) \right\} \right. \\ \left. + \text{PS}_2^{-1} \Gamma_{Born}^P S(\Lambda) \right]. \quad (28b)$$

As before, $\text{PS}_2 = \sqrt{\lambda}/16\pi m_t$ is the two-body phase space factor. $S(\Lambda)$ is the integration of the soft gluon factor $|\mathcal{M}|_{SGF}^2$ defined in Eq. (21), i.e.

$$S(\Lambda) := (-4\pi m_t) \frac{1}{2m_t} \frac{1}{(2\pi)^5} \int \frac{d^3\vec{p}_b}{2E_b} \frac{d^3\vec{q}}{2E_H} \frac{d^3\vec{k}}{2E_g} \delta^{(4)}(p_t - q - p_b - k) |\mathcal{M}|_{SGF}^2.$$

The integration $S(\Lambda)$ was done e.g. in [14]. For completeness we list the result in Appendix B.

5 Results

For ease of comparison with the results of [5, 6] we define the following abbreviations:

$$\begin{aligned}
\hat{p}_0 &= \frac{1}{2}(1 + \epsilon^2 - y^2), & \hat{w}_0 &= \frac{1}{2}(1 - \epsilon^2 + y^2), \\
\hat{p}_3 &= \frac{1}{2}\sqrt{\lambda(1, \epsilon^2, y^2)}, & \hat{w}_3 &= \hat{p}_3, \\
\hat{p}_\pm &= \hat{p}_0 \pm \hat{p}_3, & \hat{w}_\pm &= \hat{w}_0 \pm \hat{w}_3, \\
Y_p &= \frac{1}{2} \ln \frac{\hat{p}_+}{\hat{p}_-}, & Y_w &= \frac{1}{2} \ln \frac{\hat{w}_+}{\hat{w}_-},
\end{aligned} \tag{29}$$

where the hat symbols on the scaled momenta \hat{p}_i and \hat{w}_i accentuate the fact that we are dealing with dimensionless quantities. The complete $\mathcal{O}(\alpha_s)$ results are obtained by summing the Born term, the virtual one-loop and the tree-graph contributions, i.e.

$$\begin{aligned}
\frac{d\Gamma}{d \cos \theta_P} &= \frac{1}{2}(\Gamma + P \Gamma^P \cos \theta_P) \\
&= \frac{1}{2} \left[\left(\Gamma_{Born} + \Gamma_{NLO} \right) + \left(\Gamma_{Born}^P + \Gamma_{NLO}^P \right) P \cos \theta_P \right].
\end{aligned} \tag{30}$$

The unpolarized $\mathcal{O}(\alpha_s)$ corrections are given by¹

$$\Gamma_{NLO} = \Gamma_{loop} + \Gamma_{tree} = \frac{\alpha_s}{8\pi^2} C_F m_t \left[(a^2 + b^2) G_+ + (a^2 - b^2) \epsilon G_- + ab G_0 \right] \tag{31}$$

with the coefficient functions

$$\begin{aligned}
G_+ &= \hat{p}_0 \mathcal{H} + \hat{p}_0 \hat{p}_3 \left[\frac{9}{2} - 4 \ln \left(\frac{4\hat{p}_3^2}{\epsilon y} \right) \right] + \frac{1}{4y^2} Y_p (2 - y^2 - 4y^4) \\
&\quad + 3y^6 - 2\epsilon^2 - 2\epsilon^4 + 2\epsilon^6 - 4y^2\epsilon^2 - 5y^2\epsilon^4, \\
G_- &= \mathcal{H} + \hat{p}_3 \left[6 - 4 \ln \left(\frac{4\hat{p}_+^2}{\epsilon y} \right) \right] + \frac{1}{y^2} Y_p (1 - y^2 - 2\epsilon^2 + \epsilon^4 - 3y^2\epsilon^2), \\
G_0 &= -6 \hat{p}_0 \hat{p}_3 \ln \epsilon,
\end{aligned} \tag{32}$$

where

$$\begin{aligned}
\mathcal{H} &= 4\hat{p}_0 \left[\text{Li}_2(\hat{p}_+) - \text{Li}_2(\hat{p}_-) - 2 \text{Li}_2 \left(1 - \frac{\hat{p}_-}{\hat{p}_+} \right) + Y_p \ln \left(\frac{4y\hat{p}_3^2}{\hat{p}_+^2} \right) - Y_w \ln \epsilon \right] \\
&\quad + 2Y_w (1 - \epsilon^2) + \frac{2}{y^2} \hat{p}_3 (1 + y^2 - \epsilon^2) \ln \epsilon.
\end{aligned} \tag{33}$$

¹This result is written in the same form as in [6].

The polarized $\mathcal{O}(\alpha_s)$ corrections are given by

$$\begin{aligned}
\Gamma_{NLO}^{pol} &= \Gamma_{loop}^P + \Gamma_{tree}^P \\
&= \frac{\alpha_s}{8\pi^2} m_t C_F \left\{ -3(a^2 + b^2) \hat{p}_3^2 \ln \epsilon + ab \left[\frac{1}{4} \left(-11 + 28y - 16y^2 - 8y^3 + 7y^4 \right. \right. \right. \\
&\quad \left. \left. \left. + \epsilon^2(4 + 8y - 14y^2) + 7\epsilon^4 \right) + \left(2 - 9y^2 + y^4 - \epsilon^2(4 + 3y^2) + 2\epsilon^4 \right) \frac{\hat{p}_3}{y^2} Y_p \right. \right. \\
&\quad \left. \left. + 8\hat{p}_3^2 \ln \left(\frac{1-y}{(1-y)^2 - \epsilon^2} \right) + \left(3 - 3y^2 + 2\epsilon^2(4 + y^2) - 2\epsilon^4 \right) \ln \left(\frac{1-y}{\epsilon} \right) \right. \right. \\
&\quad \left. \left. + \frac{8\hat{p}_3^2 \hat{w}_0}{y^2} \ln \epsilon + 4\hat{p}_0 \hat{p}_3 \left(2\text{Li}_2 \left(1 - \frac{1-y}{\hat{p}_-} \right) - 2\text{Li}_2 \left(1 - \frac{1-y}{\hat{p}_+} \right) \right. \right. \right. \\
&\quad \left. \left. \left. - \text{Li}_2(\hat{w}_-) + \text{Li}_2(\hat{w}_+) + 2 \ln \left(\frac{(1-y^2) - \epsilon^2}{\epsilon^2} \right) Y_p \right) \right. \right. \\
&\quad \left. \left. \left. - (2 + y^4 - \epsilon^2(3 + 2y^2) + \epsilon^4) \left(2\text{Li}_2(y) - \text{Li}_2(\hat{w}_-) - \text{Li}_2(\hat{w}_+) \right) \right] \right\}. \quad (34)
\end{aligned}$$

As mentioned before the IR- and mass singularities cancel in the sum of the one-loop and the tree-graph contributions.

Next we discuss various limiting cases for the unpolarized and polarized rates, which, among others, serve to check on the correctness of our results. We have checked that our $m_b \neq 0$ results for the unpolarized rate agree with those given in [6]. We do not, however, agree with the $m_b \neq 0$ results of [7].

The limit $m_{H^+} \rightarrow 0$ is of interest since, according to the Goldstone equivalence theorem, the unpolarized and polarized rates for $t \rightarrow H^+ + b$ become related to the unpolarized and polarized longitudinal rates of $t \rightarrow W^+ + b$ in the limit $m_{H^+}, m_{W^+} \rightarrow 0$. For model 1 and $\tan \beta = 1$ in the $m_{H^+} \rightarrow 0$ limit one has

$$\begin{aligned}
\lim_{m_{H^+} \rightarrow 0} \Gamma &= \frac{m_t^3 G_F}{8\pi \sqrt{2}} |V_{tb}|^2 (1 - \epsilon^2)^3 \left\{ 1 + \frac{\alpha_s}{\pi} C_F \frac{1 + \epsilon^2}{1 - \epsilon^2} \left[\frac{5 - 22\epsilon^2 + 5\epsilon^4}{4(1 - \epsilon^4)} - 2 \ln \epsilon \ln(1 - \epsilon^2) \right. \right. \\
&\quad \left. \left. - 2\text{Li}_2(1 - \epsilon^2) - 2 \frac{1 - \epsilon^2}{1 + \epsilon^2} \ln \left(\frac{1 - \epsilon^2}{\epsilon^2} \right) - \frac{4 - 5\epsilon^2 + 7\epsilon^4}{(1 - \epsilon^2)(1 - \epsilon^4)} \ln \epsilon \right] \right\}, \quad (35a)
\end{aligned}$$

$$\begin{aligned}
\lim_{m_{H^+} \rightarrow 0} \Gamma^P &= \frac{m_t^3 G_F}{8\pi \sqrt{2}} |V_{tb}|^2 (1 - \epsilon^2)^3 \left\{ 1 + \frac{\alpha_s}{\pi} C_F \frac{1}{1 - \epsilon^2} \left[-\frac{3}{4}(5 + \epsilon^2) - 2(1 + \epsilon^2) \ln \epsilon \ln(1 - \epsilon^2) \right. \right. \\
&\quad \left. \left. - 2(1 - \epsilon^2) \ln \left(\frac{1 - \epsilon^2}{\epsilon^2} \right) - \frac{4 + 5\epsilon^2}{1 - \epsilon^2} \ln \epsilon + (1 - 2\epsilon^2) \text{Li}_2(1 - \epsilon^2) \right] \right\}. \quad (35b)
\end{aligned}$$

We have checked that expressions Eqs. (35a) and (35b) agree exactly with the $m_{W^+} \rightarrow 0$ limit of the corresponding longitudinal and polarized longitudinal rates in the process $t \rightarrow W^+ + b$ listed in [14]. This is nothing but the statement of the Goldstone equivalence theorem. Our unpolarized result in Eq. (35a) agrees with the corresponding $m_{H^+} \rightarrow 0$ result in [6].

For the sake of comparison with results in the literature we take both $m_{H^+} \rightarrow 0$ and $m_b \rightarrow 0$ in Eqs. (31) and (34) without the cautionary proviso of keeping the term $m_b \tan \beta$ in model 2. In both models 1 and 2 one then obtains

$$\lim_{m_{H^+} \rightarrow 0} \Gamma = \frac{m_t^3 G_F}{8\pi \sqrt{2}} |V_{tb}|^2 \cot^2 \beta \left[1 + \frac{\alpha_s}{2\pi} C_F \left(\frac{5}{2} - \frac{2\pi^2}{3} \right) \right], \quad (36a)$$

$$\lim_{m_{H^+} \rightarrow 0} \Gamma^P = \frac{m_t^3 G_F}{8\pi \sqrt{2}} |V_{tb}|^2 \cot^2 \beta \left[1 - \frac{\alpha_s}{2\pi} C_F \left(\frac{15}{2} - \frac{\pi^2}{3} \right) \right] \quad (36b)$$

which, when setting $\cot \beta = 1$, agree exactly with Eqs. (48) and (49) of [14] and the $\epsilon \rightarrow 0$ limits of Eqs. (35a) and (35b). The unpolarized rate in this limit agrees with the corresponding results in [5, 6, 8].

When m_{H^+} approaches m_t for $m_b \rightarrow 0$ one has

$$\lim_{m_{H^+} \rightarrow m_t} \frac{\Gamma}{\Gamma_{Born}} = 1 + \frac{\alpha_s}{2\pi} C_F \left[\frac{13}{2} - \frac{4\pi^2}{3} - 3 \ln(1 - y^2) \right], \quad (37a)$$

$$\lim_{m_{H^+} \rightarrow m_t} \frac{\Gamma^P}{\Gamma_{Born}^P} = 1 + \frac{\alpha_s}{2\pi} C_F [1 - \pi^2 - 3 \ln(1 - y^2)] \quad (37b)$$

where the $\tan \beta$ dependence has disappeared by dividing out the relevant Born terms. For the unpolarized rate the limiting expression agrees with the corresponding limit given in [6].

Finally, we consider the limit $m_b \rightarrow 0$ keeping the charged Higgs mass finite. This results in very compact expressions for the unpolarized and polarized rates. Due to the

smallness of the bottom quark mass and the fact that the bottom quark mass corrections are of $O(m_b^2/m_t^2)$ the $m_b \rightarrow 0$ formulae give quite good approximations to the exact formulae for Higgs masses as long as the Higgs mass is not close to the top quark mass.

One obtains

$$\begin{aligned} \lim_{m_b \rightarrow 0} \Gamma &= \frac{m_t}{16\pi} (1-y^2)^2 (a^2+b^2) \left\{ 1 + \frac{a^2-b^2}{a^2+b^2} \frac{2\epsilon}{1-y^2} + \frac{\alpha_s}{2\pi} C_F \left[\frac{9}{2} - \frac{2\pi^2}{3} - \frac{4y^2}{1-y^2} \ln y \right. \right. \\ &\quad \left. \left. + \left(\frac{2-5y^2}{y^2} - 4 \ln y \right) \ln(1-y^2) - 4\text{Li}_2(y^2) + \frac{(a-b)^2}{a^2+b^2} 3 \ln \epsilon \right] \right\}, \end{aligned} \quad (38a)$$

$$\begin{aligned} \lim_{m_b \rightarrow 0} \Gamma^P &= \frac{m_t}{16\pi} (1-y^2)^2 2ab \left\{ 1 + \frac{\alpha_s}{2\pi} C_F \left[-\frac{11-6y-7y^2}{2(1+y)^2} + \frac{1+2y^2}{(1-y^2)^2} \frac{\pi^2}{3} \right. \right. \\ &\quad \left. \left. + \frac{2-9y^2+y^4}{(1-y^2)y^2} \ln(1+y) + \frac{2-5y^2}{y^2} \ln(1-y) - 4\text{Li}_2(y) \right. \right. \\ &\quad \left. \left. + \frac{8+4y^4}{(1-y^2)^2} \text{Li}_2(-y) - \frac{(a-b)^2}{2ab} 3 \ln \epsilon \right] \right\}. \end{aligned} \quad (38b)$$

Again we have checked that the $m_b \rightarrow 0$ limit of the unpolarized rate agrees with the corresponding result of [6]. Note that the seemingly mass singular terms proportional to $\ln \epsilon$ in Eq. (38a) and (38b) are not in fact mass singular, since they are multiplied by the factor $(a-b)^2$, which is proportional to m_b^2 in both models 1 and 2. Although the contributions proportional to $(\epsilon^2 \ln \epsilon)$ formally vanish for $m_b \rightarrow 0$, they can become numerically quite large for $m_b = 4.8$ GeV in model 2, depending, of course, on the value of $\tan \beta$. This can be seen by calculating the ratios of the coupling factor expressions that multiply the $\ln \epsilon$ term in Eqs. (38a) and (38b). In model 1 one has $(a-b)^2/(a^2+b^2) = 2\epsilon^2/(1+\epsilon^2)$ and $(a-b)^2/(2ab) = 2\epsilon^2/(1-\epsilon^2)$, whereas in model 2 one has $(a-b)^2/(a^2+b^2) = 2\epsilon^2 \tan^4 \beta/(1+\epsilon^2 \tan^4 \beta)$ and $(a-b)^2/(2ab) = 2\epsilon^2 \tan^4 \beta/(1-\epsilon^2 \tan^4 \beta)$. In model 1 the $\ln \epsilon$ contribution is negligible but not in model 2. For example, in model 2 one finds $(a-b)^2/(a^2+b^2) = 1.77$ and $(a-b)^2/(2ab) = -2.31$ for $\tan \beta = 10$. With a little bit of algebra one finds that the NLO corrections in model 2 are in fact dominated by the $(\epsilon^2 \ln \epsilon)$ contributions for larger values of $\tan \beta$ as also noted in [6]. This is evident in Figs. 4a and 4b where the radiative corrections to the Born term rate can be seen to be as large as -50% compared to the $\approx -10\%$ expected from the corresponding corrections in the decay $t \rightarrow W^+ + b$ [14]. Note, though, that the radiative corrections become much smaller if one uses the running bottom quark mass $\bar{m}_b(m_t) = 1.79$ GeV, i.e. $\epsilon^2 \ln \epsilon = -0.00048$ instead of the fixed pole mass $m_b = 4.8$ GeV, i.e. $\epsilon^2 \ln \epsilon = -0.00271$.

We now turn to a more detailed discussion of our numerical results on the radiative corrections to the unpolarized rates and the polarization asymmetry in model 1 and 2.

We start our discussion with model 1. As input values for our numerical evaluation we use $m_b = 4.8 \text{ GeV}$ and $m_t = 175 \text{ GeV}$ as in the case of Born term. The strong coupling constant is evolved from $\alpha_s(M_Z) = 0.1175$ to $\alpha_s(m_t) = 0.1070$ using two-loop running. Fig. 2a shows that the radiative corrections lower the model 1 rate by approximately 10% over the whole range of $y = m_{H^+}/m_t$. The radiative corrections in Fig. 2b are of similar size but cannot be discerned at the scale of the figure. The radiative corrections to the polarized rate are of similar size and go in the same direction, which means that the radiative corrections to the polarization asymmetry are quite small. This can be seen in Fig. 3, which shows that the radiative corrections to the polarization asymmetry are indeed quite small and lower α_H only by $\approx 2\%$. No value of $\tan\beta$ is given in Fig. 3, since in model 1 the polarization asymmetry does not depend on $\tan\beta$ at LO and NLO, and, in fact, at any order in α_s .

Figs. 4a and 4b show that in model 2 the radiative corrections are substantial, which is mostly due to the $\epsilon^2 \ln\epsilon$ contribution discussed above. They reduce the LO rate by $\approx 50\%$ over much of the shown y and $\tan\beta$ ranges. The barely visible dotted curves in Figs. 4a and 4b are drawn using the “kinematical” $m_b \rightarrow 0$ approximations Eqs. (9a) and (9b) (LO) and Eqs. (38a) and (38b) (NLO). In these equations the bottom quark mass has been set to zero whenever the scale of m_b is set by m_t as in the kinematical factors and not by $m_t \cot^2\beta$ as in the coupling factors. As Fig. 4 shows, the “kinematical” $m_b \rightarrow 0$ approximation is an excellent approximation for both the unpolarized and polarized rate.

In Fig. 5 we show that in model 2 the radiative corrections to the LO Born term result are substantial and reduce the size of the polarization asymmetry by $\approx 25\%$ over much of the range of the Higgs mass. The $m_b \rightarrow 0$ approximation is quite good except in the endpoint region. At the scale of Fig. 5 the $m_b \neq 0$ corrections are barely visible. In Fig. 5b we fix the mass of the charged Higgs boson at $m_{H^+} = 120 \text{ GeV}$ and vary $\tan\beta$ between 0 and 30. The LO zero position $\tan\beta = \sqrt{m_t/m_b} = 6.04$ is shifted upward by approximately one unit by the radiative corrections. The radiative corrections can be seen to become quite small for the larger $\tan\beta$ values. The radiative corrections are largest around the zero position of $\tan\beta$ at $\tan\beta \approx 7$.

6 Concluding remarks

We have calculated the $O(\alpha_s)$ radiative corrections to polarized top quark decay into a charged Higgs and a bottom quark in two variants of the two-Higgs-doublet model. We have checked our unpolarized results against known results and found agreement. Using the same techniques we have calculated the polarized rate. Further, we have compared our polarized results with the corresponding polarized results in the decay $t \rightarrow W^+ + b$

appealing to the Goldstone equivalence theorem. Because of our numerous cross-checks we are quite confident that our new results on the polarized rates are correct. We have found very compact $O(\alpha_s)$ expressions for the unpolarized and polarized rates in $m_b = 0$ limit, which can be usefully employed to scan the predictions of the 2HDM $(m_{H^+}, \tan\beta)$ parameter space.

We have found that a measurement of the polarization asymmetry in the decay of a polarized top quark into a charged Higgs and a bottom quark $t(\uparrow) \rightarrow b + H^+$ can discriminate between the two variants of the two-Higgs-doublet model investigated in this paper. In model 1 the polarization asymmetry does not depend on $\tan\beta$ and stays very close to $\alpha_H = 1$ for a large range of charged Higgs mass values. This is different in model 2, in which the polarization asymmetry strongly depends on the values of $\tan\beta$ and the charged Higgs mass and can vary between $\alpha_H = 1$ and $\alpha_H = -1$ depending on the parameter values. The radiative corrections to the polarization asymmetry are quite small ($\approx 2\%$) in model 1. Again this is different in model 2 where the radiative corrections to the polarization asymmetry are important and can become as large as 25%.

Acknowledgements: A. Kadeer acknowledges the support of the DFG (Germany) through the Graduiertenkolleg ‘‘Eichtheorien’’ at the University of Mainz. M. C. Mauser was partly supported by the DFG (Germany) through the Graduiertenkolleg ‘‘Eichtheorien’’ at the University of Mainz and by the BMBF (Germany) under contract 05HT9UMB/4. M. C. Mauser would also like to thank K. Schilcher for his support.

A Loop integrals

A detailed discussion of the one-loop integrals can be found in e.g. Sec. 4 of [18].

The two-point one-loop scalar integral²:

$$\begin{aligned}
 B_0(q, m_t, m_b) &: = \frac{\mu^{4-D}}{i\pi^2} \int \frac{d^D k}{(2\pi)^{D-4}} \frac{1}{[(p_t - k)^2 - m_t^2][(p_b - k)^2 - m_b^2]} \\
 &= \frac{1}{\omega} - \gamma_E + 2 + \ln \frac{4\pi\mu^2}{m_t^2} + \frac{1 - y^2 - \epsilon^2}{y^2} \ln \epsilon + \frac{2\hat{p}_3}{y^2} Y_p. \tag{39}
 \end{aligned}$$

²Note that $q = p_t - p_b$, $q^2 = m_{H^+}^2$ and $m_t > m_b + m_{H^+}$.

The three-point one-loop scalar integral:

$$\begin{aligned}
C_0(q, m_t, m_t, m_b, m_g) &:= \frac{\mu^{4-D}}{i\pi^2} \int \frac{d^D k}{(2\pi)^{D-4}} \frac{1}{[(p_b - k)^2 - m_b^2] [(p_t - k)^2 - m_t^2] (k^2 - m_g^2)} \\
&= -\frac{1}{m_t^2} \frac{1}{2\hat{p}_3} \left\{ (\ln \epsilon + Y_p) (Y_p + 2Y_w) + (\ln \epsilon - 2 \ln \Lambda) Y_p - \text{Li}_2\left(1 - \frac{\hat{w}_-}{\hat{w}_+}\right) + \text{Li}_2\left(1 - \frac{\hat{p}_- \hat{w}_-}{\hat{p}_+ \hat{w}_+}\right) \right\}.
\end{aligned} \tag{40}$$

The three-point one-loop vector integral:

$$\begin{aligned}
C^\mu(q, m_t, m_t, m_b, m_g) &:= \frac{\mu^{4-D}}{i\pi^2} \int \frac{d^D k}{(2\pi)^{D-4}} \frac{k^\mu}{[(p_b - k)^2 - m_b^2] [(p_t - k)^2 - m_t^2] (k^2 - m_g^2)} \\
&= C_1 p_t^\mu + C_2 p_b^\mu.
\end{aligned} \tag{41}$$

where

$$C_1 = \frac{1}{m_t^2} \frac{1}{y^2} \left[\ln \epsilon + (1 - y^2 - \epsilon^2) \frac{Y_p}{2\hat{p}_3} \right], \tag{42}$$

$$C_2 = -\frac{1}{m_t^2} \frac{1}{y^2} \left[\ln \epsilon + (1 + y^2 - \epsilon^2) \frac{Y_p}{2\hat{p}_3} \right]. \tag{43}$$

B Integration of the soft gluon factor

$$\begin{aligned}
S(\Lambda) &:= (-4\pi m_t) \frac{1}{2m_t} \frac{1}{(2\pi)^5} \int \frac{d^3 \vec{p}_b}{2E_b} \frac{d^3 \vec{q}}{2E_H} \frac{d^3 \vec{k}}{2E_g} \delta^{(4)}(p_t - q - p_b - k) |\mathcal{M}|_{SGF}^2 \\
&= \frac{\alpha_s}{4\pi} C_F \left(4\hat{p}_3 \left[\ln\left(\frac{4\hat{p}_3^2}{\epsilon y \Lambda}\right) - 2 \right] - 2(1 - \epsilon^2) Y_w + 2\epsilon^2 Y_p + 2\hat{p}_0 \left\{ 2\text{Li}_2\left(1 - \frac{\hat{p}_-}{\hat{p}_+}\right) \right. \right. \\
&\quad \left. \left. - \text{Li}_2\left(1 - \frac{\hat{w}_-}{\hat{w}_+}\right) + \text{Li}_2\left(\frac{2\hat{p}_3}{\hat{p}_+ \hat{w}_+}\right) - Y_p \left[2 \ln\left(\frac{4\hat{p}_3^2}{\hat{p}_+ \hat{w}_+ \Lambda}\right) - Y_p + 1 \right] \right\} \right),
\end{aligned} \tag{44}$$

where the soft gluon (or eikonal) factor $|\mathcal{M}|_{SGF}^2$ is defined in Eq. (21).

C Basic integrals for the tree-graph phase space integrations

Details of the calculation of basic integrals can be found in [14]. Note that our notation differs from the notation in [14].

$$R(-1) = -2\hat{p}_3 + 2\hat{p}_3 \ln\left(\frac{2\hat{w}_+\hat{p}_3}{y^2\epsilon_2}\right) - (1 - \epsilon^2 + y^2) Y_w, \quad (45)$$

$$R(0) = \frac{1}{2} \ln \left[\frac{(1-y)^2 - \epsilon^2}{(1+y)^2 - \epsilon^2} \right] + \ln\left(\frac{\hat{w}_+}{y\epsilon_2}\right), \quad (46)$$

$$R(0,0) = (1-y)^2 - \epsilon^2, \quad (47)$$

$$R(0,-1) = \hat{p}_3 (1 - \epsilon^2 + y^2) - 2y^2 Y_w, \quad (48)$$

$$R(-1,0) = 2 \ln\left(\frac{1-y}{\epsilon}\right), \quad (49)$$

$$R(-1,-1) = -2\hat{p}_3 + 2(1-y^2) Y_p - 2y^2 Y_w, \quad (50)$$

$$R(-2,0) = \epsilon^{-2} - (1-y)^{-2}, \quad (51)$$

$$R(-2,-1) = \frac{2\hat{p}_3}{\epsilon^2} - \frac{2}{1-y^2} \left[(1+y^2) Y_p + y^2 Y_w \right], \quad (52)$$

$$R(1,0) = \frac{(1-y)^4}{2} - \frac{\epsilon^4}{2}, \quad (53)$$

$$S(0) = \text{Li}_2(\hat{w}_+) - \text{Li}_2(\hat{w}_-) - 2\text{Li}_2\left(1 - \frac{\hat{p}_-}{\hat{p}_+}\right) + 2 \ln\left(\frac{2\hat{w}_+\hat{p}_3}{y^2\epsilon_2}\right) Y_p - 2Y_p^2 + 2Y_w \ln \epsilon, \quad (54)$$

$$S(1) = \frac{1}{\hat{p}_3} \left\{ \text{Li}_2\left(-\frac{y}{\hat{w}_+}\right) - \text{Li}_2\left(-\frac{y\hat{p}_-}{\hat{p}_+\hat{w}_+}\right) + \ln\left(\frac{2\hat{p}_3}{y\epsilon_2}\right) Y_p - Y_p^2 \right\}, \quad (55)$$

$$S(0,-1) = -\frac{1}{4} \left[(1-y)^2 - \epsilon^2 \right] \left[\epsilon^2 - (3-y)(1+y) \right] - (1-y^4) \ln\left(\frac{1-y}{\epsilon}\right) \\ + 2y^2 \left[2\text{Li}_2(y) - \text{Li}_2(\hat{w}_-) - \text{Li}_2(\hat{w}_+) \right] + 2(1 - \epsilon^2 + y^2) \hat{p}_3 Y_p, \quad (56)$$

$$S(0,0) = 2(\hat{p}_3 - \epsilon^2 Y_p - y^2 Y_w), \quad (57)$$

$$S(0,1) = \text{Li}_2(\hat{w}_-) + \text{Li}_2(\hat{w}_+) - 2\text{Li}_2(y), \quad (58)$$

$$S(1, 0) = \frac{\hat{p}_3}{2} (1 + \epsilon^2 + 5y^2) - \epsilon^4 Y_p - y^2 (2 + y^2) Y_w, \quad (59)$$

$$S(1, 1) = \epsilon^2 - (1 - y)^2 + 2(1 - y^2) \ln\left(\frac{1 - y}{\epsilon}\right) - 4\hat{p}_3 Y_p \\ + (1 + y^2) \left[\text{Li}_2(\hat{w}_-) + \text{Li}_2(\hat{w}_+) - 2\text{Li}_2(y) \right], \quad (60)$$

$$S(2, 1) = \frac{1}{4} [\epsilon^2 - (1 - y)^2] [4 + \epsilon^2 + (1 - y)^2 + 8y^2] + 3(1 - y^4) \ln\left(\frac{1 - y}{\epsilon}\right) \\ - (1 + 4y^2 + y^4) \left[2\text{Li}_2(y) - \text{Li}_2(\hat{w}_-) - \text{Li}_2(\hat{w}_+) \right] \\ - 2\hat{p}_3 (3 + \epsilon^2 + 3y^2) Y_p. \quad (61)$$

References

- [1] G. Mahlon and S. Parke, Phys. Rev. **D55** (1997) 7249.
- [2] D. Espriu and J. Manzano, **hep-ph/0209030**.
- [3] S. Parke and Y. Shadmi, Phys. Lett. **B387** (1996) 199.
- [4] M. Fischer, S. Groote, J.G. Körner, M.C. Mauser and B. Lampe, Phys. Lett. **B451** (1999) 406.
- [5] A. Czarnecki and S. Davidson, Phys. Rev. **D47** (1993) 3063.
- [6] A. Czarnecki and S. Davidson, Phys. Rev. **D48** (1993) 4183.
- [7] C.S. Li et al., Phys. Lett. **B285** (1992) 137.
- [8] J. Liu and Y.P. Yao, Phys. Rev. **D46** (1992) 5196.
- [9] J. Reid, G. Tupper, G. Li, and M.S. Samuel, Z. Phys. **C51** (1991) 395.
- [10] C.S. Li and T.C. Yuan, Phys. Rev. **D42** (1990) 3088.
- [11] C.S. Li and T.C. Yuan, Phys. Rev. **D47** (1993) 2156(E).
- [12] J. Liu and Y.P. Yao, Report No. **UM-TH-90-09** (1990) (unpublished).

- [13] J. Liu and Y.P. Yao, Int. J. Mod. Phys. **A6** (1991) 4925.
- [14] M. Fischer, S. Groote, J.G. Körner, and M.C. Mauser,
Phys. Rev. **D65** (2002) 054036, **hep-ph/0101322**.
- [15] J.F. Gunion, H.E. Haber, G.L. Kane and S. Dawson,
The Higgs Hunter's Guide, (Addison-Wesley, Reading, MAA, 1990).
- [16] Particle Data Group, W. M. Yao *et al*, Journal of Physics **G33** (2006) 1.
- [17] E. Braaten and J.P. Leveille, Phys. Rev. **D22** (1980) 715.
- [18] A. Denner, Fortschr. Phys. **41** (1993) 307.